J. Phys. Chem. Solids Vol. 50, No. 3, pp. 297–308, 1989
Printed in Great Britain.

0022-3697/89 $3.00 + 0.00

MAGNETISM OF IRON–SULFUR TETRAHEDRAL FRAMEWORKS IN COMPOUNDS WITH THALLIUM I. CHAIN STRUCTURES

D. WELZ,† P. DEPPE, W. SCHAEFER,‡ H. SABROWSKY§ and M. ROSENBERG
Institut fuer Experimentalphysik VI, Ruhr-Universitaet, D-4630 Bochum 1, F.R.G.

(*Received* 21 *April* 1988; *accepted* 5 *October* 1988)

Abstract—The ternary iron sulfides, monoclinic $TlFeS_2$ (linear tetrahedral chains) and orthorhombic $Tl_3Fe_2S_4$ (folded tetrahedral chains), have been investigated by means of magnetic susceptibility measurements, powder neutron diffraction, and Mössbauer spectroscopy. Both compounds exhibit three-dimensional antiferromagnetic order with Néel temperatures of 190(10) and 90(5) K, respectively. The low-temperature magnetic structures have been obtained and the moment values are 1.85(6) μ_B for $TlFeS_2$ and 1.5(2) μ_B for $Tl_3Fe_2S_4$. The magnitude and the coupling of moments in the Fe–S tetrahedral frameworks are seen to be strongly influenced by direct Fe–Fe interactions for edge-sharing tetrahedra, while the Fe–S bond may be described as ionic. The Fe–Fe interaction apparently goes along with a metallic state, permitting an intermediate valence ($Fe^{2.5+}$) in the folded chain compound.

Keywords: Ternary iron sulfides, tetrahedral chain structures, magnetic susceptibility, powder neutron scattering, spin arrangements, magnetic moments, Mössbauer spectroscopy.

1. INTRODUCTION

The thallium iron sulfides, which are the subject of the present study, belong to a quite general class of ternary compounds of an electropositive metal A, a transition-metal M, and a chalcogen X, for which a common structural principle is manifest in spatially extended anisotropic M–X frameworks held in place by the intervening A-atoms. Characteristically, the members of this class of compounds exhibit polar bonds between an anionic M–X framework and A-cations as well as covalent or metallic behavior throughout and confined to the framework [1, 2].

For a given combination of elements A, M and X, often a whole family is found of related compounds differing in stochiometry, an instructive example of which is presented by the well studied Ba-Fe–S system with about a dozen members identified to date [3]. Passing from one composition to the next, a change in cation content (or a substitution of chemically distinct cations) may be balanced by a change in the average transition metal valence, but an increased electron donation will eventually break up the anionic units and leave frameworks of lower dimension. Such dismantling may proceed from M–X layers or networks through multiple or single chains to clusters or segments of chains, and it terminates with isolated simple M–X units. Even phases with "infinitely adaptive" structures have been described such as $Ba_{1+x}Fe_2S_4$, where a continuous variation of stoichiometry is accomplished by an incommensurate Ba-filling between parallel Fe–S chains [4].

The thallium iron sulfides known today have been crystallographically characterized during the past decade and their frameworks, shown in Fig. 1, all involve edge-sharing iron-centered sulfur tetrahedra. There are three such compounds, namely monoclinic $TlFeS_2$ (space group C_{2h}^3 ($C2/m$), IT No. 12 [5]), known to mineralogists as raguinite and featuring rectilinear chains of tetrahedra [Fig. 1(a)] [6, 7], orthorhombic $Tl_3Fe_2S_4$ (D_{2h}^{16} ($Pnma$), No. 62), where the chains take on a zigzag shape to accommodate additional Tl [Fig. 1(b)] [8], and a continuous series of $TlFe_xS_2$ phases for $1.3 \leqslant x \leqslant 1.8$ based on the tetragonal $ThCr_2Si_2$ structure (D_{4h}^{17} ($I4/mmm$), No. 139) with planar sheets of tetrahedra only incompletely occupied by Fe [Fig. 1(c)] [7, 8]. Finally, the rare mineral picotpaulite should be mentioned, which has been described as orthorhombic $TlFe_2S_3$ [9], but to our knowledge no determination of the structure has been undertaken until now.

Concerning the previous work on these sulfides, some remarks are in order. The folded chain compound $Tl_3Fe_2S_4$ has so far been assigned a monoclinic cell (space group C_{2h}^5 ($P2_1/c$), No. 14) with $a = 13.03$, $b = 11.14$, $c = 7.383$ Å and $\beta = 124.5°$ [8], but within the given accuracy this can be transformed to orthorhombic axes as $a' = c$, $b' = a + c$, $c' = b$ (vectorial addition) where $b' = 10.73$ Å. In Table 1 the (hitherto unpublished) atomic positions obtained from a single

† Present address: Institute for Solid State Physics, Univerity of Tokyo, Roppongi, Minato-ku, Tokyo 106, Japan.

‡ Mineralogisches Institut, Universitaet Bonn.

§ Institut fuer anorganische Chemie I, Ruhr-Universitaet Bochum.

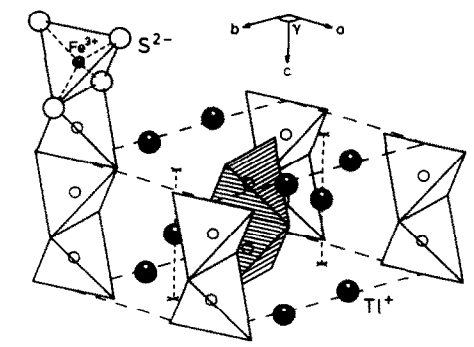

$TlFeS_2$ I 1 1 2/m

a = 6,83 Å b = 10,51 Å c = 5,31 Å γ = 98,6°

(a)

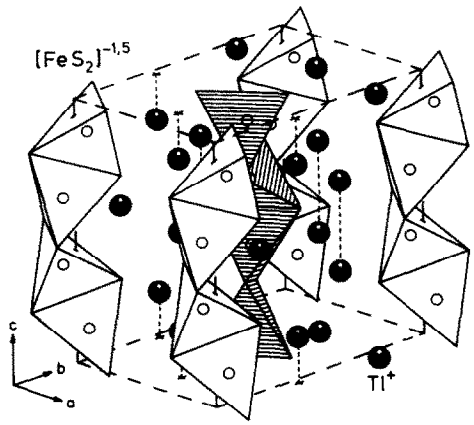

$Tl_3Fe_2S_4$ P $2_1/n$ $2_1/a$ $2_1/m$

a = 7,38 Å b = 11,14 Å c = 10,73 Å

(b)

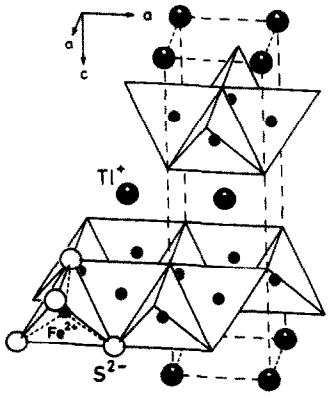

$TlFe_xS_2$ I4/mmm

a = 3,75 Å c = 13,4 Å

(c)

Fig. 1. Crystallographic structures of (a) monoclinic $TlFeS_2$, (b) orthorhombic $Tl_3Fe_2S_4$ and (c) tetragonal $TlFe_xS_2$ ($1.3 \leqslant x \leqslant 1.8$) with partly vacant Fe-sites. Note that non-standard settings have been chosen to depict $TlFeS_2$ and $Tl_3Fe_2S_4$.

crystal X-ray analysis [10] are listed in the new coordinates (D_{2h}^{16} (*Pnma*), No. 62). $Tl_3Fe_2S_4$ thus turns out to be isomorphic with $Na_3Fe_2S_4$ [11] with all Fe in equivalent (8*d*)-positions of the *Pnma* space group. An interesting aspect is that the Fe-sites should then be assigned a non-integer average formal valence of +2.5, which for the corresponding sodium sulfide and selenide was recently confirmed by Mössbauer spectra showing a single state intermediate between Fe^{2+} and Fe^{3+} [12].

The presence of vacant tetrahedra in tetragonal $TlFe_xS_2$, in contrast to isostructural $TlCo_2S_2$ or $TlNi_2S_2$ which have consistently been described as stoichimetric [7, 13], naturally raises the question of vacancy order. From X-ray data showing peak splitting and weak superstructure reflections for concentrations around $x = 1.5$ (1.40–1.55), Zabel and Range [14] derived an ordered vacancy arrangement of the type found for the orthorhombic compounds $A_2M_3S_4$ with A = (Rb, Cs) and M = (Mn, Co, Zn) [15]. With respect to the remaining concentrations, they assumed two different kinds of statistical distribution for phases below and above $x = 1.65$ [14]. We are of the opinion, however, that their assertion of an "orthorhombic symmetry yet tetragonal metric" for low x [14] remains unclear, and that no explanation is offered for the observed abrupt reduction in the c-axis for x exceeding 1.65.

This being the preceding state of research, the present study of the thallium iron sulfides by susceptibility measurements, powder neutron diffraction and Mössbauer spectroscopy has been undertaken to provide the lacking magnetic characterization, but also to improve on the crystallographic description for the range of tetragonal layered phases since, compared with X-ray diffraction, the neutron scattering factors here offer a greater sensitivity to ordered vacancy arrangements. A short preliminary account of some results has been given in [16].

For reasons of length, the present detailed report is divided in two, and the remainder of this communication only deals with the chain phases $TlFeS_2$ and $Tl_3Fe_2S_4$. The results for the layered tetragonal $TlFe_xS_2$ compounds are to be presented in a separate publication referred to as Part II.

Table 1. Atomic positions for the folded chain compound $Tl_3Fe_2S_4$ at room temperature from single crystal X-ray analysis [8], transformed to a standard *Pnma* orthorhombic setting†

Atom	Position	*x*	*y*	*z*
Tl (1)	4*c*	0.410	0.25	0.276
Tl (2)	8*d*	0.452 (0)	0.077 (2)	0.635 (1)
Fe	8*d*	0.461 (2)	0.124 (2)	0.966 (4)
S (1)	4*c*	0.119	0.25	0.668
S (2)	4*c*	0.240	0.25	0.022
S (3)	8*d*	0.143 (1)	0.053 (3)	0.377 (2)

† The errors in parentheses indicate the mismatch of formerly inequivalent positions. The dimensions of the *Pnma* cell are $a = 7.38$, $b = 10.73$ and $c = 11.14$ Å.

2. SAMPLE PREPARATION AND CHARACTERIZATION

The compositions $TlFeS_2$ and $Tl_3Fe_2S_4$ were prepared by fusing metallic thallium fragments with proper amounts of powdered iron and sulfur in evacuated and sealed silica tubes at temperatures finally raised to 1050°C, followed by rapid cooling from the molten state through exposure of the tubes to free air or immersion in water. The resulting ingots consisted of needle-shaped crystallites with metallic luster, graphite colored for $Tl_3Fe_2S_4$ and tending to violet for $TlFeS_2$, in agreement with the published descriptions [6–8]. Grinding in a ball mill showed the compounds to be ductile and the crystallites to be easily split. The powdered samples were checked by taking X-ray Guinier diagrams, which established them to consist essentially of the respective intended phase; the most noticeable impurity contribution was from layered $TlFe_xS_2$ in the $Tl_3Fe_2S_4$ samples.

Conflicting with the initial characterization, the powder of the folded chain compound $Tl_3Fe_2S_4$, being kept without particular precautions in a small glass container with a snap-on lid, after several months showed, among others, clear scattering contributions from the linear chain phase $TlFeS_2$. The transformation was visibly accompanied by a blackening of the grains, which should be attributed to extrusion of Tl with subsequent oxidation, and the mechanism may be similar to the topotactic oxidation to $NaFeS_2$ (and accompanying hydration) reported for $Na_3Fe_2S_4$ exposed to ambient humidity [17]. The process was typically found to be completed after six months when $Tl_3Fe_2S_4$ was no longer detected. Although the measurements presented in the following have been carried out on newly prepared material, an appreciable contamination will still be evident.

The transformation appears to be particularly fast for the fine grained samples used in the Mössbauer measurements (Section 5), as expected for a reaction proceeding from the surface, but it also seems to occur for the bulk material. One preparation of $Tl_3Fe_2S_4$ was left sealed in its silica tube at room temperature for a period of four months and then showed only diffuse X-ray reflections and an ill-resolved, broadened Mössbauer spectrum. Thus, even the possibility of a metastable state at room temperature has to be considered.

We also tried to synthesize picotpaulite, $TlFe_2S_3$, by the same method, but this simply led to a phase mixture with a substantial contribution from the linear chain phase $TlFeS_2$.

3. MAGNETIC SUSCEPTIBILITY MEASUREMENTS

The magnetic susceptibility of the compounds was measured in a Faraday balance in the range from 4.2 K to room temperature, using an applied field of 1 T (10 kG). For both chain phases, the small susceptibility values obtained preclude the possibility of a ferromagnetic state and imply an internal compensation of magnetic moments. A slight general decrease with temperature is noted, but there are no indications of magnetic phase transitions in the investigated temperature range, in striking contrast to the demonstration by Mössbauer spectroscopy (Section 5) of magnetic transitions at 190(10) K and 90(5) K†, respectively.

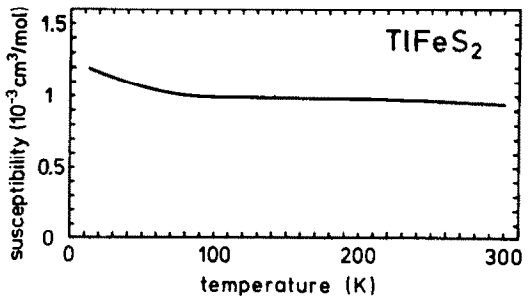

Fig. 2. Molar magnetic susceptibility of $TlFeS_2$ in an applied field of 1 T (10 kG).

Figure 2 shows the molar susceptibility of the linear chain phase $TlFeS_2$. A similarly unrevealing behavior has been reported for the structurally related alkali–metal compounds $KFeS_2$ and $RbFeS_2$ [18], for which magnetic phase transitions are known to occur at similar temperatures (250(1) and 188(1) K, respectively [2]). The flat susceptibility curves thus appear to be characteristic of this type of linear chain compound and, according to [18], they should be taken as an indication of pronounced one-dimensional antiferromagnetism. Indeed, an antiferromagnetic alteration of moments along the chains in $TlFeS_2$ will be derived from the neutron scattering data (Section 4), and a small ratio of the inter- to intra-chain exchange interactions, $J'/J = 8.6 \cdot 10^{-3}$, has been obtained from inelastic neutron scattering for the K-compound [19].

For one-dimensional antiferromagnets, theoretical considerations predict slowly varying susceptibility curves passing through a broad maximum [20]. If the suceptibility of $9 \cdot 10^{-4}$ cm^3 mol^{-1} obtained for $TlFeS_2$ is identified with the theoretical value as the susceptibility maximum for an ($S = 1$)-Heisenberg chain [20], and if 1.85 μ_B is taken for the magnetic moment (Section 4), the exchange integral may be calculated as $J = 0.088\, N(g\mu_B)^2/\chi \cong 10$ meV and the maximum should appear around $2.70\, J/k \cong 300$ K. Due to impurity contributions, however, the actual susceptibility may be smaller, whence both of these values should only be taken for lower bounds. The estimate for the J-value nevertheless is of the order of the intra-chain exchange integral in $KFeS_2$, $J = 20.8$ meV, directly obtained from neutron scattering [19].

† Figures attached in parentheses specify an uncertainty in the last decimal place.

In contrast to the conformity of results for the various linear chain compounds, the Na-analogues of the folded chain compound, for comparable applied fields, show a sudden increase in the susceptibility that coincides with the Mössbauer transition (at 149 and 179 K for $Na_3Fe_2S_4$ and $Na_3Fe_2Se_4$, respectively) [12]. A corresponding transition should have been noticed in our susceptibility data for $Tl_3Fe_2S_4$, in spite of a much higher background contribution ($6 \cdot 10^{-2}$ cm^3 mol^{-1}) which may largely be due to impurity phases. (Instead, a hardly discernable flat susceptibility minimum appears around 90 K.)

From the field dependence of the susceptibility below the transition temperature, the Na-compounds have been characterized as weakly ferrimagnetic, but no reason has been suggested for the appearance of a small net moment [12] (from the $Na_3Fe_2S_4$ data [12] we obtain about $7 \cdot 10^{-4}\ \mu_B$ per Fe-atom). With crystallographically equivalent Fe-sites in the given structure [Fig. 1(b)] and with the corresponding unique magnetic Mössbauer spectra [12], the residual moment values suggest a slightly imperfect antiparallelism of identical moments in the Na-compounds, whereas a full compensation seems to be achieved for $Tl_3Fe_2S_4$.

4. NEUTRON DIFFRACTION

Powder neutron diffraction patterns at room and cryogenic temperatures (16 K) were recorded by means of a position-sensitive detector (^{6}Li glass scintillator) installed on the two axis diffractometer SV7 at the FRJ-2 reactor of KFA Juelich [21]. A neutron wavelength of 1.433(2) Å was used, and the typical acquisition time was 12 h for one diagram. The patterns were subjected to Rietveld analysis [22], i.e. a direct fit with a superposition of peak profiles without the need for a previous peak separation. The background was manually defined (and later optimized), and the refinement was carried out with one common isotropic temperature factor, fixed site occupancies, and with a correction for a preferred orientation of the crystallites included [22].

In Fig. 3(a), neutron diffraction diagrams are shown for the linear chain compounds $TlFeS_2$. All peaks of the room temperature pattern can be indexed in terms of the known chemical cell [6, 7], which confirms the sample to be essentially free of impurity phases. The Rietveld refinement (R-value 9.5†) reveals a considerable preferred orientation of the needle-shaped crystallites, and the resulting cell and positional parameters, listed in Table 2, are in close agreement with the values obtained from X-ray diffraction [7]. From the neutron diffraction data in particular, a slight dimerization of iron along the chain axis [$y_{Fe} = 0.254(1)$] is seen that reflects the asymmetry of the surrounding Tl-positions.

In the low-temperature pattern, two additional reflections can be recognized [Fig. 3(a)], which require non-integer indices with respect to the chemical cell, (0, 1, 1/2) and (−2, 1, 3/2) for the standard $C12/m1$ setting (Table 2), and (−1/2, 1/2, 1) and (1/2, 3/2, 1) for the $I112/m$ setting [Fig. 1(a)]. Since the remaining pattern is unchanged except for shifts due to lattice contraction, the new reflections should be attributed to a three-dimensional magnetic order of iron moments at 16 K. As also required from the susceptibility data (Section 3), the appearance of non-integer indices implies that the order is not simply ferromagnetic; a transformation from the $I112/m$ axes to a face-centered cell of twice the original volume, $a' = a - b$, $b' = a + b$, $c' = c$ (vectorial addition), leads to integer indices with $h + l$ even, (1, 0, 1) and (−1, 2, 1), and suggests a B-centered magnetic occupation of the new cell.

From the fact that the Fe-atoms of a single chain are related by inversion symmetry and that separate chains transform into each other by translation, a strictly collinear spin arrangement is expected with no restriction on the absolute spin direction. Since the chain axis passing through the Fe-atoms, however, is a two-fold rotation axis, the absolute orientation should either be parallel or normal to the chain direction. For the structurally related alkali-metal sulfides $KFeS_2$ and $RbFeS_2$, neutron diffraction has further established collinear spin structures with antiferromagnetic alteration along the chains [2, 23]. When antiferromagnetic chains are assumed for $TlFeS_2$ as well as among the possible relative orientations in the planes normal to the chain axis, only the configuration depicted in Fig. 4(a) is compatible with the observed reflections.

For this spin configuration, the observed peak intensities are at variance with a spin direction parallel to the chain axis, while for orientations within the monoclinic plane a Rietveld refinement leads to a satisfactory solution for the orientation shown in Fig. 4(a) (magnetic R-value 12.9, nuclear R-value 8.5). The resulting magnetic moment is 1.85(6) μ_B, and the angle with the a-axis is −57(10)° for the $I112/m$ cell [or +60(10)° for the standard $C12/m1$ cell]. In obtaining these values, the Fe^{3+} magnetic form factor calculated by Watson and Freeman [24] has been used.

An analysis of systematic extinction for the $TlFeS_2$ spin configuration shows that, in terms of the above defined face-centered cell, only magnetic reflections of the types (o, e, o) and (e, o, e) with $l \neq 0$ may occur, where e and o denote "even" and "odd", respectively. Thus all magnetic reflections are distinct from the nuclear ones for the face-centered cell,

† The R-value is defined as [22]

$$R = 100 \sum_i \left[S_i^2(\text{obs}) - \frac{1}{c} S_i^2(\text{calc}) \right] \Big/ \sum_i S_i^2(\text{obs}),$$

where $1/c$ is a common scale factor, S_i^2(obs) are the suitably separated observed and S_i^2(calc) the calculated peak intensities, and the summation includes all reflections contributing to the diagram.

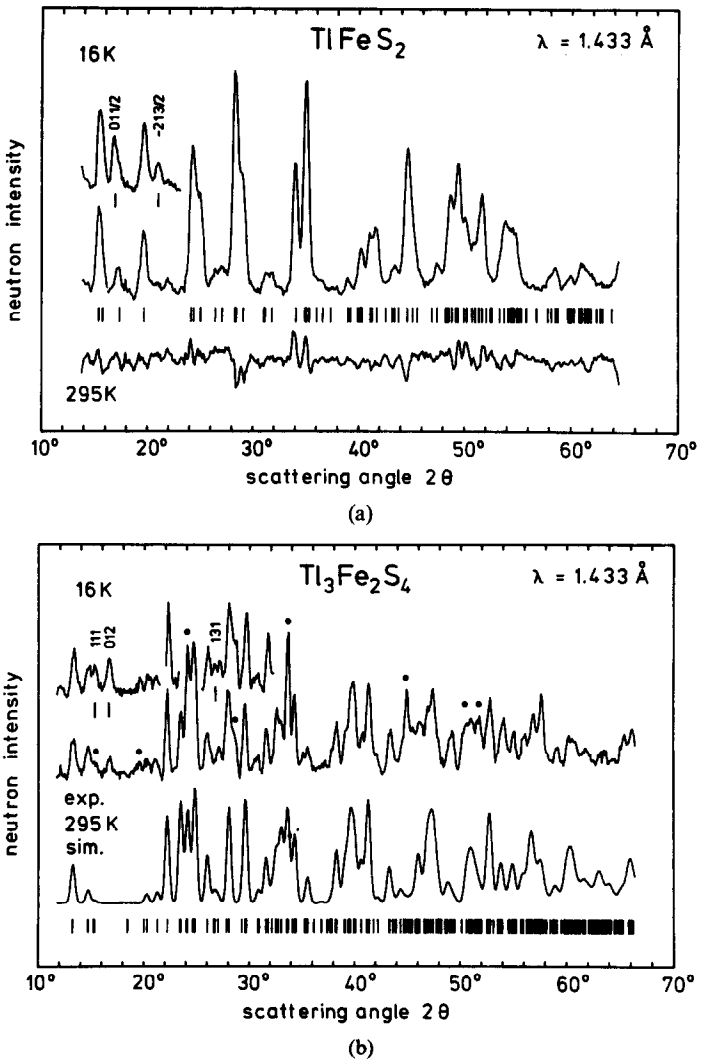

Fig. 3. Background-corrected neutron diffraction patterns for (a) $TlFeS_2$ and (b) $Tl_3Fe_2S_4$ at room temperature, and with additional magnetic reflections at 16 K (low-angle region only); the indices refer to the standard $C12/m1$ and *Pnma* setting, respectively. Also shown are the positions of expected reflections, the residual error for the Rietveld refinement ($TlFeS_2$) and a pattern simulated from the X-ray structural data of Table 1 ($Tl_3Fe_2S_4$). Impurity contributions in the experimental pattern are marked by dots.

(e, e, e) and (o, o, o). Furthermore, the nearly equal spacing of Fe-atoms along the chains effectively causes the extinction of all magnetic reflections with l even, and just two observed reflections remain for scattering angles 2θ below 24°. Conversely, for ferromagnetically ordered chains, the nearly degenerate z-position of Fe would have led to extinction for l odd, in contradiction to observation. Thus the above made assumption of antiferromagnetic chains is justified.

Apart from the occurrence of antiferromagnetic chains, the spin structure obtained for $TlFeS_2$ differs from those of $KFeS_2$ and $RbFeS_2$, where the monoclinic angle (of about 113°) is formed between the chain axis and the shorter of the remaining cell axes (space group C_{2h}^6 ($C2/c$), IT No. 15 [5]). In these compounds, the spin direction is slightly tilted from the chain axis (by about 13°) and the arrangement in the complementary planes is ferromagnetic [2, 23]. For $KFeS_2$, the magnetic moment is given as

Table 2. Atomic positions for the linear chain compound $TlFeS_2$ at room temperature obtained from a Rietveld refinement of neutron powder diffraction data (R-value 9.5)†

Atom	Position	x	y	z
Tl	4*i*	0.034 (1)	0	0.359 (1)
Fe	4*g*	0	0.254 (1)	0
S (1)	4*i*	0.259 (3)	0	0.299 (3)
S (2)	4*i*	0.416 (4)	0	0.092 (4)

† The setting is $C12/m1$ and the cell data are $a = 11.68(2)$, $b = 5.32(1)$, $c = 10.53(2)$ Å and $\beta = 144.60(1)°$.

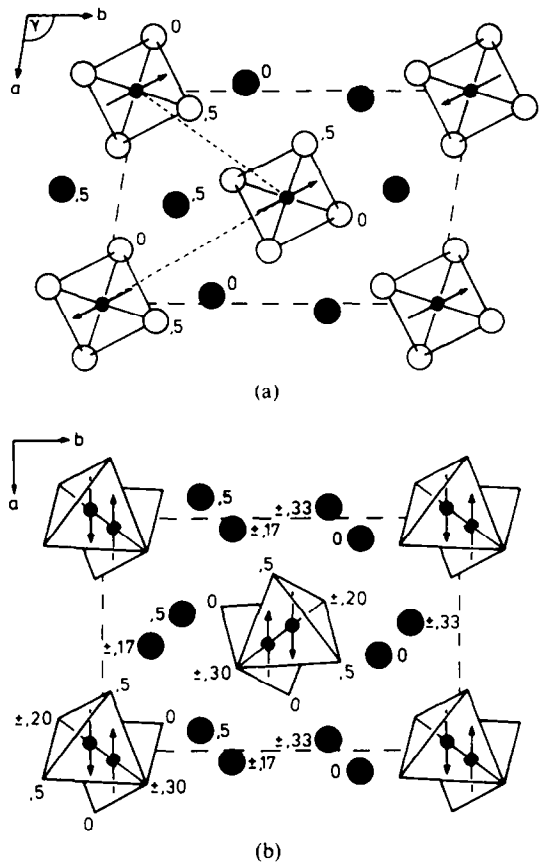

Fig. 4. Projections of the crystallographic cell of (a) $TlFeS_2$ and (b) $Tl_3Fe_2S_4$ with the orientation of magnetic moments obtained from neutron diffraction. The moment values are (a) 1.85(6) μ_B and (b) 1.52(2) μ_B. The non-standard settings of Fig. 1 are used and the numbers indicate the height of atoms above the basal plane.

2.43(3) μ_B [23], somewhat higher than for the present $TlFeS_2$ (values given in [2] correspond to 1.9(3) μ_B for $KFeS_2$ and 1.8(3) μ_B for $RbFeS_2$). The finding of spin directions both perpendicular and nearly parallel to the chains demonstrates that in these compounds no local magnetic anisotropy is operative, as expected from a $3d^5$-spherical electronic configuration for a formal Fe-valence of +3.

Yet, the magnetic moments of the order 2 μ_B in the chain structures obviously fall substantially short of the Fe^{3+} ionic value (5 μ_B), which might be taken as an indication of considerable covalency in the Fe–S bonding. The moment values, however, fall equally short of the values for zinc blende type tetrahedral sulfides like $CuFeS_2$ (Fe^{3+}, 3.85 μ_B [25]) or cubic FeS (Fe^{2+}, 3.45 μ_B [26]), where only corner-sharing Fe–S tetrahedra are found. Thus, the reduced moment values in the chain structures give evidence of sizeable direct interactions of neighboring iron atoms in frameworks of edge-sharing tetrahedra. This may be readily understood by noting that the Fe–Fe distance here amounts to merely about 2.7 Å as compared with 2.48 Å in the bcc iron metal.

Another interesting comparison involves $CsFeS_2$, which is orthorhombic at room temperature (D_{2h}^{25} (*Immm*), IT No. 71), but undergoes a simultaneous first-order structural and magnetic transition at 70 K [27]. Apart from the monoclinic angle γ of 98.52(1)°, the atomic arrangement of $TlFeS_2$ in the *I*112/*m* setting [Fig. 1(a)] represents only a slight distortion of the room temperature phase of the Cs-compound. Without monoclinic distortion, however, the exchange interactions between the center chain and each corner chain of the cell should be identical, which is incompatible with the magnetic structure of $TlFeS_2$ [Fig. 4(a)]. If similar inter-chain exchange constants are present in the orthorhombic Cs-phase, the structural transition may take place to circumvent the magnetic frustration. The reason for this and the peculiar magnetic structure of $TlFeS_2$ should be suspected in a dominating antiferromagnetic interaction along the shorter of the monoclinic axes in Fig 4(a).

In Fig. 3(b), neutron diffraction diagrams for the folded chain compound $Tl_3Fe_2S_4$ are presented together with a synthetic pattern calculated from the X-ray structural data of Table 1. Comparison of the room temperature diagram and the simulated pattern shows an overall correspondence which includes all major reflections, but it also reveals scattering contributions that are not accounted for. A Rietveld refinement consequently converges for structural parameters that represent a deviation from the X-ray data and, moreover, does not result in a satisfactory description of the experimental pattern (*R*-value 18.6).

Some of the plainly conflicting scattering contributions are indicated in Fig. 3(b) and, in accordance with the X-ray characterization (Section 2), they can largely be identified with the layered phases $TlFe_xS_2$ (Fig. 2 of Part II) and, less noticeable, the linear chain compound $TlFeS_2$ [Fig. 3(a)]. Upon exclusion of regions with major suspected contamination (comprising about 30% of the diagram), the refinement is noted to improve, but some of the sulfur positions are left unstable, most probably because of a remaining impurity interference and the smaller scattering length of sulfur (8.79, 9.54, and 2.85 fm for Tl, Fe, and S, respectively [28]). Since we do not believe that the resulting parameters constitute an improvement on the X-ray data of Table 1, they are not listed here. The neutron diffraction pattern of the present sample, however, provides strong evidence in favor of the *Pnma* structural model for the folded chain compound, in particular with respect to the Fe- and S-positions which here significantly enter the scattering intensities.

In the low-temperature diagram [Fig. 3(b)], again additional reflections appear for an otherwise unchanged pattern, indicating the occurrence of three-dimensional magnetic order at 16 K without any crystallographic transition. For the present orthorhombic structure, equivalent relations of the center

chain with each corner chain [Fig. 4(b)] make a magnetic supercell unlikely even for an antiferromagnetic spin configuration in the normal planes, and the magnetic reflections recognized in Fig. 3(b) can indeed be indexed on the *Pnma* chemical cell as (1, 1, 1) [possibly (0, 2, 0)], (0, 1, 2) and (1, 3, 1) [possibly (2, 0, 2)]. The unambiguous presence of the (0, 1, 2) reflection in particular violates the systematic extinction associated with the (x, y, z) to $(-x + 1/2, y + 1/2, z + 1/2)$ diagonal glide operation which allows only even $k + l$ for reflections with $h = 0$, whence the spin orientation must be differrent for positions related by this operation.

To proceed with the deduction of the spin structure, we again make the assumption of an essentially collinear configuration, as expected for an ordered state dominated by exchange interactions among nearest neighbors. For reasons of symmetry, i.e. because of the presence of mirror and glide planes, the common spin direction should then coincide with one of the cell axes. Furthermore, from the result for the linear chain structure, it appears reasonable to assign an antiparallel orientation to the Fe-pairs in the straight chain segments, which here are the only direct neighbors related by inversion symmetry. This assumption is supported by the absence in the susceptibility data (Section 3) of a residual moment for the ordered state, implying a complete magnetic compensation. One is then left with the possibility either of fully alternating chains and an antiferromagnetic arrangement in the normal planes or of a parallel spin orientation at the bends and a ferromagnetic arrangement in the planes—both for spin directions along any of the orthorhombic cell axes.

A calculation of theoretical reflection intensities for each model shows that only the second one with the spins pointing along the a-axis may account for the observed magnetic pattern; this spin configuration is depicted in Fig. 4(b). From a Rietveld refinement, a moment value of $1.5(2)\,\mu_B$ is obtained (magnetic R-value 62.1). To eliminate any disturbing influence of (non-magnetic) impurity phases, the fit has been performed on the 2θ regions from 12° to 22° and from 26° to 27.5° after subtraction of the room temperature pattern (adjusted for lattice expansion) with the amplitude factor and preferred orientation correction taken over from a separate fit on the full pattern with the major impurity regions excluded. In view of the present precision, the details of the actual magnetic form factor should be immaterial, and thus the Fe^{3+} spherical factor [24] has been used. The calculated intensities satisfactorily reproduce those of the observed magnetic reflections: three additionally predicted reflections, (0, 3, 0) (31%), (1, 1, 3) (36%) and (0, 3, 2) (33%), are probably masked by nuclear scattering or lost in noise, while all others amount to at most 13% of the (1, 1, 1) magnetic intensity.

Yet it must be noted that, owing to the need for assumptions, poor statistics and the possible influence of magnetic impurities, the present result for the spin structure of $Tl_3Fe_2S_4$ is to be taken with some reserve. In particular, a related collinear configuration with spins in the x-direction, namely parallel orientation in the straight chain segments and reversal at the bends, leads to similar intensities and cannot be ruled out on grounds of the diffraction data alone (though it may fit the observed pattern slightly less well). Other collinear arrangements, however, can confidently be excluded. A significant deviation from collinear orientation is regarded as highly improbable, but this again cannot be decided from the present data. [A deviation, if any, must be compatible with a single-component magnetic Mössbauer spectrum (Section 5).]

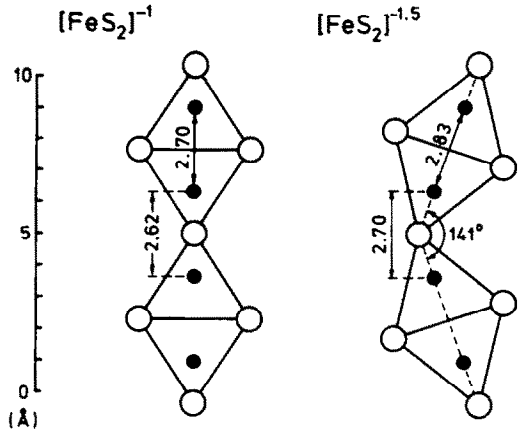

Fig. 5. Geometry of the linear Fe–S chains in $TlFeS_2$ and of the folded chains in $Tl_3Fe_2S_4$. Distances and angles are calculated from the structural data of Tables 2 and 1, respectively.

A remarkable feature of the above derived spin structure of $Tl_3Fe_2S_4$ is the finding of a ferromagnetic arrangement at the bends of the folded chains. For $TlFeS_2$ and the related alkali-metal compounds, the magnetic structures invariably show antiferromagnetic interactions, but they all involve Fe^{3+} and linear chains. In the present case, a different interaction should then arise from a change in the bonding configuration for $Fe^{2.5+}$ or from the folding of the chains (Fig. 5). This in particular may take the form of either a changed direct Fe–Fe overlap or a different mediation by sulfur in a superexchange dominated interaction. The importance of such Fe–S–Fe superexchange and its antiferromagnetic nature are established by the high Néel temperatures for blende type $CuFeS_2$ (T_N above room temperature [25]) and cubic FeS ($T_N = 234$ K [26]), where tetrahedral angles ($\approx 109.5°$) are formed at the common S-corners. Since the Fe–S–Fe angle at the bends of the present folded chains [73(2)°] hardly differs from the angle for ideal straight chains ($\sim 70.5°$), a change of sign appears most unlikely, and the ferromagnetic coupling should be attributed to a change in Fe–Fe overlap. The different Fe–Fe separations of 2.83 Å in

the straight segments and of 2.70 Å across the bends (Fig. 5) may be related to this.

One may wonder what the implications are for the Na-analogue of the folded chain compound for which, assuming the crystallographic structure to be maintained, the ferrimagnetic moment reported for the ordered state [12] should be explained as a deviation from a perfectly collinear spin orientation (Section 3). Such may indeed be expected as an effect of local anisotropy forces, but a strictly antiparallel orientation in the straight chain segments should still cause a net zero moment as in the case of $Tl_3Fe_2S_4$. Thus, either the low-temperature crystallographic symmetry or the magnetic symmetry of the Na- and the Tl-compound should be different from each other.

5. MÖSSBAUER SPECTROSCOPY

Mössbauer spectra were recorded in standard transmission geometry for absorber temperatures between 4.2 and 295 K, employing a $^{57}Co(Rh)$ source of nominally 25 mCi kept at room temperature. An electromechanical drive was used to generate a sinusoidal or alternating constant acceleration of the source, and the data from the proportional counter were synchronously accumulated in a 512-channel analyzer and later folded into 256 channels. The strong γ-absorption by thallium dictated the use of finely ground powder (dispersed in an inert carrier) for the absorber, and necessitated acquisition times of a few days. The spectra were analyzed by means of least-squares fitting with an appropriate combination of lorentzian lines. In the following, the isomer shift values are given with respect to the room temperature $^{57}Co(Rh)$ source where the shift for metallic iron is -0.11 mm s^{-1} [29]; values quoted from the literature have been converted accordingly.

The spectra taken for the chain phases at 295, 100 ($Tl_3Fe_2S_4$ only) and 4.2 K are shown in Fig. 6. As expected from the corresponding neutron diffraction results, they are paramagnetic and magnetically split, respectively, and thus confirm the occurrence of magnetic transitions below room temperature. The data from the least-squares analysis are presented in Table 3. From measurements at intermediate temperatures, the transition temperatures were localized at 190(10) K for $TlFeS_2$ and at 90(5) K for $Tl_3Fe_2S_4$.

For the linear chain compound $TlFeS_2$, the low-temperature spectrum [Fig. 6(a)] may reasonably well be analyzed using the standard first-order treatment

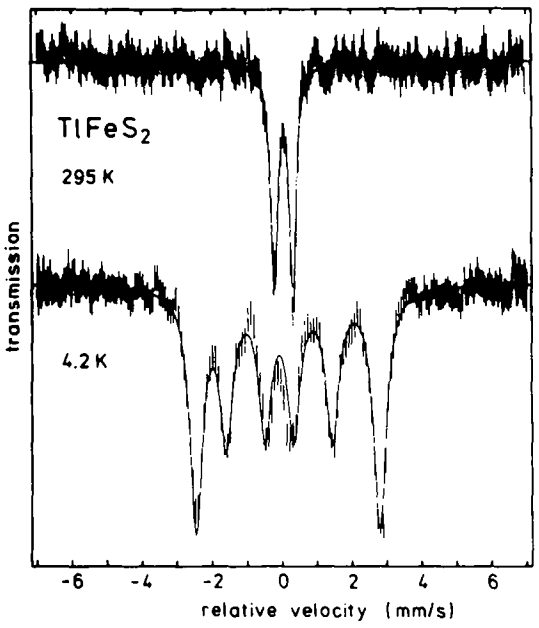

(a)

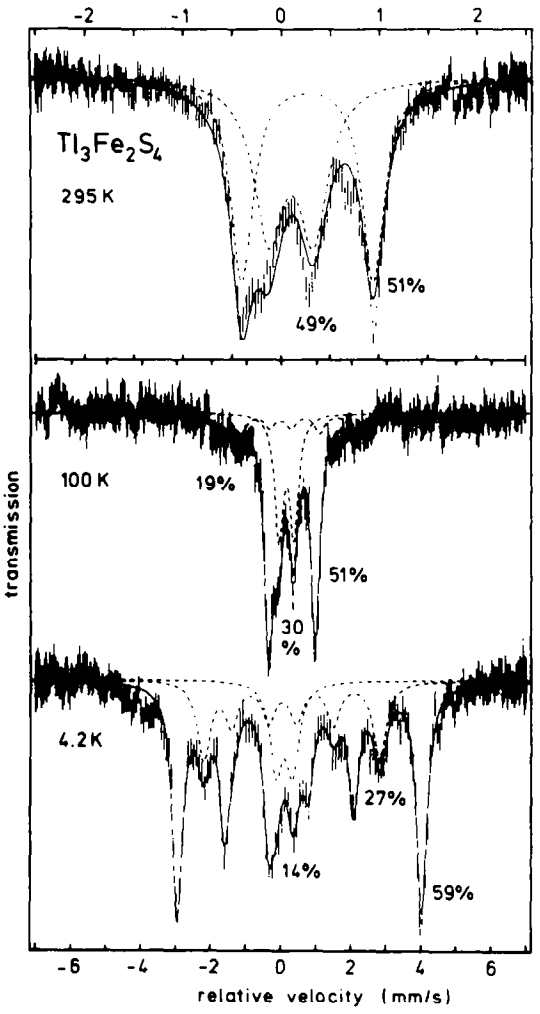

(b)

Fig. 6. Mössbauer spectra of (a) $TlFeS_2$ and (b) $Tl_3Fe_2S_4$ at room temperature, 100 K (b only). and 4.2 K. Additional contributions in the $Tl_3Fe_2S_4$ spectra (dashed) are attributed to a partial decay into $TlFeS_2$. The component percentages are given and, for clarity, the main component is not drawn separately for 100 and 4.2 K. The spectrum at 100 K has been taken with a different sample.

Table 3. Mössbauer least-squares data for $TlFeS_2$ and $Tl_3Fe_2S_4$†

		$TlFeS_2$	$Tl_3Fe_2S_4$	
i.s.	(295 K)	+0.05 (1)	+0.27 (1)	mm s^{-1}
i.s.	(100 K)	—	+0.37 (1)	mm s^{-1}
i.s.	(4.2 K)	+0.05 (1)	+0.40 (1)	mm s^{-1}
q.s.	(295 K)	0.53 (1)	1.35 (3)	mm s^{-1}
q.s.	(100 K)	—	1.52 (2)	mm s^{-1}
q.s.	(4.2 K)	+0.25 (1)	—	mm s^{-1}
hff	(4.2 K)	163 (3)	201 (4)	kG

† Listed are the isomer shift (i.s.) relative to $^{57}Co(Rh)$, the magnetic hyperfine field (hff), and the quadrupole splitting and first-order shift (q.s.) in the paramagnetic and magnetic spectra (4.2 K), respectively. No first order shift is given for $Tl_3Fe_2S_4$ because of the strong quadrupole interaction.

of the electric quadrupole interaction. The effect of the electric field gradient (efg) may then be written [30]

$$\Delta E_Q^p = \tfrac{1}{2}\sqrt{1+\eta^2/3}\, eQV_{zz} \qquad (1)$$

for the splitting in the paramagnetic spectrum and

$$\Delta E_Q^m = \tfrac{1}{4}(3\cos^2\theta - 1 + \eta \sin^2\theta \cos 2\phi) eQV_{zz} \qquad (2)$$

for the first-order shift of the outer doublet relative to the inner lines in the magnetic spectrum. Here, V_{zz} is the main diagonal component of the efg tensor, $\eta = (V_{xx} - V_{yy})/V_{zz}$ is the asymmetry parameter, and the polar and azimuthal angles θ and ϕ specify the magnetic orientation relative to the efg principal axes.

In the magnetic spectrum of $TlFeS_2$, we find a quadrupole shift ΔE_Q^m of +0.25(1) mm s^{-1}, representing half of the splitting for the paramagnetic state, 0.53(1) mm s^{-1} (Table 3). For a presumably nearly spherical Fe^{3+} located in an isolated and ideally symmetric Fe–S tetrahedral chain, the low-temperature efg should not significantly differ from the room temperature value, no deviation from cylindrical symmetry should appear, and the major principal axis should coincide with the chain axis. Given the first two conditions, the Mössbauer data imply either $\theta \cong 35°$ for $eQV_{zz} > 0$, or $\theta \cong 90°$ for $eQV_{zz} < 0$. In the actual $TlFeS_2$ environment, the chain axis passing through Fe shows only a two-fold rotation symmetry, whence the major efg principal axis may be either parallel or perpendicular to the axis, but negligible deviations from the ideal chain geometry as well as a calculation of the lattice efg with ionic charges +1, +3, and −2 for Tl, Fe, and S suggest it remains along the chain axis. To be consistent with the perpendicular magnetic orientation obtained from neutron scattering (Section 4), of the above possibilities then $\theta = 90°$ and $eQV_{zz} < 0$ must be taken.

This choice is (tentatively) supported by the indication in the magnetic spectrum [Fig. 6(a)] of higher order shifts that cause the innermost lines to be less separated than expected from the first-order fitted curve, whereas for $eQV_{zz} > 0$ the separation should be increased. (To assess the effect of higher order corrections one may compare Figs 6 and 11 of Ref. 31 for a ratio $R = 0.53/1.10 = 0.48$ of the paramagnetic splitting to the separation of the magnetic lines 2 and 3 or 4 and 5.) For the linear chain phase $TlFeS_2$, we thus have $eQV_{zz}/2 = -0.53(1)$ mm s^{-1}, and using $Q = +0.19 \cdot 10^{-24}$ cm^2 [32], an efg of $V_{zz} = -0.27 \cdot 10^{18}$ V cm^{-2} with negligible asymmetry and pointing along the chain axis is obtained.

A small positive isomer shift of +0.05(1) mm s^{-1} is found for $TlFeS_2$ (Table 3), which is somewhat lower than, albeit still compatible with, the values generally given for ionic Fe^{3+} ($\sim +0.3$ mm s^{-1} [29]). It is, however, also compatible with a covalent or metallic state of iron [29], as implied by the reduced magnetic moment value (Section 4). The usual decrease with temperature, expected from second-order Doppler shifts due to thermal motion, is not reflected in the data of Table 3. This is likely to be a consequence of the higher order effects neglected in the least-squares analysis.

The hyperfine parameters of $TlFeS_2$ conform well with Mössbauer results for the related alkali-metal compounds [33]. In particular, $\eta \cong 0$ and a negative eQV_{zz} aligned with the chain axis were also derived from measurements on a $KFeS_2$ single crystal [34], and the magnetic hyperfine field and moment of $KFeS_2$ nicely scale with the values obtained here. This may be expressed as a common hyperfine coupling constant for Fe^{3+} in tetrahedral coordination to sulfur: from the $KFeS_2$ data at 77 K (215(5) kG [33] and 2.37(3) μ_B [23]) one obtains 91(3) kG/μ_B, while for $TlFeS_2$ one has 88(3) kG/μ_B from 163(3) kG and 1.85(6) μ_B at 4.2 and 16 K, respectively. Since the magnetic direction for the K-compound nearly coincides with the chain axis whereas for the Tl-compound it points perpendicular, the magnetic hyperfine interaction is seen to be virtually isotropic and should essentially be equated to the core-polarization Fermi contact term for spherical Fe^{3+}. The value of the coupling constant is typical of solid state Fe^{3+} and falls somewhat short of values calculated for the free ion, e.g. 126 kG/μ_B [35], due to the presence of a counteracting 4*s*-contribution.

From the Mössbauer spectra of the folded chain compound $Tl_3Fe_2S_4$ [Fig. 6(b)], multiple contributions originating from chemically distinct iron sites are evident, which are at variance with the equivalent Fe-positions in a *Pnma* crystallographic structure. Three subspectra can be separated at low temperatures: in addition to a main magnetic component (59%), of which parameters are given in Table 3, we find a magnetic spectrum (27%) with a clearly distinct isomer shift [+0.19(2) mm s^{-1}] and a less well defined paramagnetic component (14%) with a similar isomer shift and a quadrupole splitting of about 0.45(5) mm s^{-1}. Apart from a slightly higher isomer shift, the latter components are reminiscent

of magnetic and paramagnetic $TlFeS_2$, respectively [Fig. 6(a)], and the analogy with the X-ray observation of the chemical decomposition of $Tl_3Fe_2S_4$ (Section 2) suggests their identification as Fe-containing intermediate or final transformation products. A small additional magnetic contribution around $-4.5\,mm\,s^{-1}$ should be ascribed to layered $TlFe_xS_2$.

The identification of the multiple Mössbauer components with separate phases is corroborated by the persistence of a magnetic $TlFeS_2$-like component in the spectrum taken at 100 K, where the main phase is already paramagnetic [Fig. 6(b)]. From the spectra, the magnetic main component is seen to transform to the outer doublet at room temperature, and for the corresponding intensities a parallel decrease has been noted with progressive decomposition of the sample. One may thus confidently take the respective Mössbauer main components alone to be representative of $Tl_3Fe_2S_4$. Apart from a somewhat smaller quadrupole splitting, their appearance closely resembles that of the recently published spectra for the sodium selenide $Na_3Fe_2S_4$ [12], and the repeated finding of single-component spectra in accordance with a *Pnma* crystallographic structure underlines the occurrence of metallic delocalization in the folded chains with equivalent Fe in an intermediate valence state.

A considerably increased content of $TlFeS_2$-like impurities [compared with the initial X-ray characterization (Section 2) and the neutron diffraction results (Section 4)] in all of the samples prepared for Mössbauer measurements suggests that the chemical decomposition of $Tl_3Fe_2S_4$ is greatly accelerated by the crushing process or by the subsequent prolonged contact of fine grains with the carrier material (silicone grease).

The comparatively strong quadrupole interaction for the folded chain compound necessitates an analysis beyond the first-order treatment embodied in eqn (2). A comparison of the peak positions extracted from the low-temperature magnetic spectrum [Fig. 6(b)] by means of least-squares fitting of independent lorentzians (-2.93, -1.59, -0.32, 0.80, 2.09 and 4.04 mm s^{-1}, about ± 0.02 mm s^{-1} each) with the theoretical patterns in Ref. 31 suggests solutions in the vicinity of $\eta = 0$ and either $\theta \cong 40°$ for $eQV_{zz} > 0$ or $\theta \cong 60°$ for $eQV_{zz} < 0$. (An estimate with the 100 K quadrupole splitting gives the ratio $R = 1.52/1.28 = 1.19$ [31].) Starting from the above values, a numerical parameter optimization with $(1 + \eta^2/3)^{1/2} eQV_{zz}/2$ constrained to the value at 100 K leads to $\theta = 49°$ and a considerable asymmetry, $\eta = 0.50$, with $\phi = 0°$ ($eQV_{zz}/2 = +1.46$ mm s^{-1}) or to $\theta = 66°$ and a negligible asymmetry ($eQV_{zz}/2 = -1.52$ mm s^{-1}), respectively. Below it will be argued in favor of the solution with positive eQV_{zz}. For both cases, however, virtually identical values result for the isomer shift ($+0.40$ mm s^{-1}) and magnetic splitting (6.46 mm s^{-1}) and are entered in Table 3. (The values differ noticeably from direct estimates from the peak positions.)

It should be noted that the magnetic orientation and the efg asymmetry parameter obtained in this way depend sensitively on the linearity of the velocity scale and thus may be subject to errors that are hard to quantify. The scatter of results obtained from different spectra allows estimating uncertainties of about $\pm 2°$ for θ and ± 0.1 for η.

A clear increase in the quadrupole splitting with decreasing temperature [1.35(3) and 1.52(2) mm s^{-1} for 295 and 100 K, respectively] is seen from Table 3, corresponding to a shift from Fe^{3+}- to Fe^{2+}-like behavior and suggesting a major electronic contribution to the efg in $Tl_3Fe_2S_4$. The isomer shift falls well between typical Fe^{3+} ($+0.05$ mm s^{-1} for $TlFeS_2$) and Fe^{2+} values (about $+0.6$ mm s^{-1} for blende type cubic FeS [26]), and its temperature variation [0.27(1), 0.37(1) and 0.40(1) mm s^{-1} for 295, 100 and 4.2 K] conforms to what has to be expected from thermal second-order Doppler shifts.

The characteristically different hyperfine parameters for the linear and folded chain compounds call for a common interpretation based on the presence of metallic delocalization as reflected in the reduced magnetic moments (Section 4) and an intermediate valence state for the folded chains. Metallic Fe-3*d* bands and a substantial Fe–Fe interaction have further been directly demonstrated in a recent band structure calculation for the sheets of edge-sharing Fe–S tetrahedra in tetragonal iron monosulfide [36]. The interpretation for the present compounds may look as follows.

In the case of linear chain compounds such as $KFeS_2$ or $TlFeS_2$ with a formal Fe-valence of $+3$, we proceed from a cubic $3d^5$-configuration of Fe with the *e*-orbitals stabilized in the tetrahedral Fe–S bonding environment, where for the absence of deviations from tetrahedral symmetry no efg appears. This orbital configuration is subject to (i) energy shifts induced by Fe–Fe bonding interactions, and (ii) a polarization induced by the lattice contribution to the efg, which also largely arises from the Fe-ions in the two adjoining tetrahedra. The *z*-coordinate being taken along the chain axis, analogy with the situation for the tetragonal monosulfide [36] suggests that the Fe–Fe interaction primarily results in a splitting of the $3z^2$–r^2 orbitals and a population excess for the complementary x^2–y^2 orbital, giving rise to a positive V_{zz}. Concerning the lattice efg we expect a repopulation of orbitals at the Fermi level which overcompensates the Sternheimer type antishielding from closed shells, where the effective factor $(1 - \gamma)$ should be of the order of -10 [36]. In contrast to the effect of Fe–Fe bonding, the lattice efg will then lead to $V_{zz} < 0$, and a negative experimental net value implies that here the lattice induced polarization predominates.

In the case of the folded chain compounds like $Tl_3Fe_2S_4$, one should interpret the much larger

quadrupole splitting as the signature of an initially non-spherical atom where an excess orbital is stabilized by the deviation from cubic environmental symmetry. A clear-cut example of this is presented by $3d^6$-Fe^{2+} in the orthorhombic state of the blende type monosulfide [26]. With respect to the present Tl-compound, this interpretation is supported by the finding of one half of the quadrupole splitting that is typical of full-blown Fe^{2+} (about 3 mm s^{-1} [37]), corresponding to one half excess electron, as expected from the formal valence of +2.5. The temperature variation of the quadrupole splitting may then be attributed to thermal excitation from the stabilized orbital into unoccupied states with an energy separation of the order of 0.1 eV.

With only moderate spin splitting, as implied by the small moment values, the e-orbitals should be largely occupied and a pronounced asymmetry is only likely to arise in the t_2-manifold, which is also suggested by the geometry of the folded Fe–S chains that allows the t_2-orbitals to overlap at the bends (Fig. 5). The folding results in a loss of equivalence of the orientations normal to the local chain axis and, for the usual choice of coordinates in a tetrahedral environment, the distinct axes should be chosen as $x+y$ and $x-y$, i.e. in the plane and perpendicular to the plane defined by the Fe-loci of the chain. The non-spherical contribution may then be accounted for by either the $(xz+yz)$ or the $(xz-yz)$ symmetry adapted orbital. Since for each a major efg principal component of $+4/7|e|\langle r^{-3}\rangle$ is obtained [37], of the two sets of Mössbauer parameters, that belonging to positive V_{zz} has to be taken. For this solution, the experimentally observed angle of the major principal axis with the spin direction along the a-axis of the orthorhombic cell (49°) coincides reasonably well with the angle formed by the a-axis and the above defined plane (53°), and the excess orbital in question should be that with the lobes oriented perpendicular to this plane.

The argument may be carried on to account for an asymmetry in the efg by including the polarization effects outlined in the case of the linear chains, but here one should expect the limits of such simple model pictures. We note in conclusion that the present inference of an additional Fe–Fe interaction via t_2-overlap correlates with the finding of an exceptional ferromagnetic spin coupling at the bends of the folded chains (Section 4).

A pronounced non-spherical Fe orbital configuration in $Tl_3Fe_2S_4$ is expected to introduce orbital and dipolar hyperfine field contributions in addition to the Fermi contact term. The experimental coupling constant of 134(18) kG/μ_B [201(4) kG and 1.5(2) μ_B] indeed significantly exceeds the $3d^5$-Fe^{3+} isotropic value found for the linear chain compounds (90 kG/μ_B), and the assumption of additional contributions is warranted even in view of a possible valence-related change in the Fermi field. In this context, it is instructive to compare the well documented and extreme case of 42 kG/μ_B (145 kG and 3.45 μ_B) for the blende-type monosulfide [26].

A non-spherical electronic configuration of Fe is further expected to introduce a considerable magnetic anisotropy (e.g. a local easy axis) which is likely to affect the magnetic structure since, for the folded chain geometry, the local directions should be in conflict with a strictly collinear moment arrangement. For the isostructural sodium compounds, the closely similar Mössbauer spectra imply a similar electronic configuration (including the angle θ) irrespective of a suspected different magnetic structure (Section 4), and the corresponding anisotropy here should give rise to the minute residual magnetic moments found below the ordering temperature [12].

6. CONCLUSIONS

The results of the present magnetic characterization of the linear chain ($TlFeS_2$) and folded chain ($Tl_3Fe_2S_4$) tetrahedral framework phases in the ternary thallium–iron–sulfur system may be summarized as follows:

(i) Rather small Fe magnetic moments of 1.85(6) and 1.5(2) μ_B are obtained, respectively, falling substantially short of the values for zinc blende-type tetrahedral sulfides.

(ii) A strong antiferromagnetic intra-chain exchange leads to pronounced one-dimensional magnetic characteristics for the linear chain compounds, but evidence is found of an exceptional ferromagnetic coupling at the bends of the folded chains.

(iii) At 190(10) and 90(5) K, respectively, magnetic transitions take place that result in a three-dimensional antiferromagnetic state for the lower temperatures.

The results supplement earlier investigations of the structurally related alkali-metal compounds and may be considered typical of chain frameworks composed of edge-sharing Fe–S tetrahedra.

The magnetic properties of the compounds take their origin in the electronic structure. Here, the Mössbauer hyperfine data allow us to form a satisfactory picture of the Fe electronic configuration and bonding environment:

(i) An intermediate valence state for the folded chain phase and the substantially higher magnetic moments in the merely corner-sharing Fe–S tetrahedra of the blende-type compounds give evidence of an Fe–Fe metallic delocalization in the chains of edge-sharing tetrahedra. The significance of direct Fe–Fe interactions accounts for the strong dependence of magnetic properties on the individual structure in tetrahedral iron sulfides.

(ii) The Mössbauer results show a pronouncedly non-spherical $Fe^{2.5+}$ in the folded chains (stabilized excess orbital), while magnetically isotropic Fe^{3+} is found for the linear chain phase, suggesting an ionic description for the Fe–S bond. This conforms with an interpretation given for the blende-type cubic

monosulfide, whose properties could also be successfully explained assuming "good" high-spin Fe^{2+}-ions with only minor covalency [26].

Thus the electronic characterization of the Fe–S tetrahedral framework phases involves two aspects which form a stimulating contrast.

Acknowledgements—This work has been funded by the German Federal Minister for Research and Technology (BMFT) under contract number 03-B55B02. The authors are also indebted to A. Thimm for synthesizing the $TlFeS_2$ sample, to A. Kortenbreer for taking X-ray diffraction measurements, and to Dr P. Mueller (RWTH Aachen) for providing a copy of the Rietveld code.

REFERENCES

1. Bronger W., *Angew. Chem.* **93,** 12 (1981).
2. Bronger W. and Mueller P., *J. less-common Metals* **100,** 241 (1984).
3. Reiff W. M., Grey I. E., Fan A., Eliezer Z. and Steinfink H., *J. Solid St. Chem.* **13,** 32 (1975); Lemley J. T., Jenks J. M., Hoggins J. T., Eliezer Z. and Steinfink H., *J. Solid St. Chem.* **16,** 117 (1976); Cohen S., Kimizuka N. and Steinfink H., *J. Solid St. Chem.* **35,** 181 (1980).
4. Cohen S., Rendon Diazmiron L. E. and Steinfink H., *J. Solid St. Chem.* **25,** 179 (1978).
5. Henry N. F. M. and Lonsdale K. (Editors), *International Tables for X-ray Crystallography*, Vol. I. Kynoch Press, Birmingham (1969).
6. Klepp K. and Boller H., *Mh. Chem.* **110,** 1045 (1979).
7. Zabel M. and Range K.-J., *Z. Naturf.* **34b,** 1 (1979).
8. Sabrowsky H., Mirza J. and Methfessel Ch., *Z. Naturf.* **34b,** 115 (1979).
9. Johan Zd., Pierrot R., Schubnel H.-J. and Permingeat F., *Bull. Soc. fr. Minér. Cristallogr.* **93,** 545 (1970).
10. Mirza J., thesis, Bochum (1978).
11. Klepp K. and Boller H., *Monatsh. Chem.* **112,** 83 (1981).
12. Ensling J., Guetlich P., Spiering H. and Klepp K., *Hyperfine Int.* 28, 599 (1986).
13. Klepp K. and Boller H., *Monatsh. Chem.* **109,** 1049 (1978).
14. Zabel M. and Range K.-J., *Rev. Chim. Miner.* **17,** 561 (1980); *Rev. Chim. Miner.* **21,** 139 (1984).
15. Bronger W. and Boettcher P., *Z. anorg. allg. Chem.* **390,** 1 (1972); Bronger W. and Hendriks U., *Rev. Chim. Miner.* **17,** 555 (1980).
16. Sabrowsky H., Rosenberg M., Welz D., Deppe P. and Schaefer W., *J. Magn. Magn. Mater.* **54–57,** 1497 (1986).
17. Boller H. and Blaha H., *Monatsh. Chem.* **114,** 145 (1983).
18. Bronger W., *Z. anorg. allg. Chem.* **359,** 225 (1968).
19. Nishi M., Ito Y. and Funahashi S., *J. phys. Soc. Japan* **52,** 2210 (1983).
20. Jongh L. J. de and Miedema A. R., *Adv. Phys.* **23,** 1 (1974).
21. Schelten J., Kurz R., Naday I. and Schaefer W., *Nucl. Instrum. Meth.* **205,** 319 (1983); Schaefer W., Jansen E., Elf F. and Will G., *J. appl. Crystallogr.* **17,** 159 (1984).
22. Rietveld H. M., *J. appl. Crystallogr.* **2,** 65 (1969).
23. Nishi M. and Ito Y., *Solid St. Commun.* **30,** 571 (1979).
24. Watson R. E. and Freeman A. J., *Acta crystallogr.* **14,** 27 (1961).
25. Donnay G., Corliss L. M., Donnay J. D. H., Elliott N. and Hastings J. M., *Phys. Rev.* **112,** 1917 (1958).
26. Wintenberger M., Srour B., Meyer C., Hartmann-Boutron F. and Gros Y., *J. Physique* **39,** 965 (1978); Wintenberger M. and Buevoz J. L., *Solid St. Commun.* **27,** 511 (1978).
27. Nishi M., Ito Y. and Ito A., *J. phys. Soc. Japan* **52,** 3602 (1983); Ito Y., Nishi M., Majkrzak C. F. and Passell L., *J. phys. Soc. Japan* **54,** 348 (1985).
28. Lovesey St. W., *Theory of Neutron Scattering from Condensed Matter*, Vol. 1, p. 17. Clarendon Press, Oxford (1984).
29. Shenoy G. K. and Wagner F. E. (Editors), *Mössbauer Isomer Shifts*. North-Holland, Amsterdam (1978).
30. Abragam A., *The Principles of Nuclear Magnetism*. Clarendon Press, Oxford (1961).
31. Kuendig W., *Nucl. Instrum Meth.* **48,** 219 (1967).
32. Fuller G. H., *J. phys. Chem. Ref. Data* **5,** 835 (1976).
33. Raj D. and Puri S. P., *J. chem. Phys.* **50,** 3184 (1969); Taft C. A., Raj D. and Danon J., *J. Phys. Chem. Solids* **36,** 283 (1975); Taft C. A., Raj D. and Danon J., *J. Physique Coll.* **35,** C6-241 (1974).
34. Scorzelli R. B., Taft C. A., Danon J. and Garg V. K., *J. Phys. C* **11,** L397 (1978).
35. Watson R. E. and Freeman A. J., *Phys. Rev.* **123,** 2027 (1961).
36. Welz D. and Rosenberg M., *J. Phys. C* **20,** 3911 (1987).
37. Hartmann-Boutron F. and Imbert P., *J. appl. Phys.* **39,** 775 (1968).